



ELSEVIER

Contents lists available at ScienceDirect

Biophysical Chemistry

journal homepage: [www.elsevier.com/locate/biophyschem](http://www.elsevier.com/locate/biophyschem)

## Research Article

# Simultaneous multisite detection of quantal release from PC12 cells using micro graphitic-diamond multi electrode arrays

Giulia Tomagra<sup>a,\*</sup>, Claudio Franchino<sup>a</sup>, Alberto Pasquarelli<sup>c</sup>, Emilio Carbone<sup>a</sup>, Paolo Olivero<sup>b</sup>,  
Valentina Carabelli<sup>a</sup>, Federico Piccolo<sup>b</sup>

<sup>a</sup> Department of Drug and Science Technology, NIS Inter-departmental Centre, University of Torino, Corso Raffaello 30, 10125 Torino, Italy

<sup>b</sup> Department of Physics, NIS Inter-departmental Centre, University of Torino, Italian Institute of Nuclear Physics, via Giuria 1, 10125 Torino, Italy

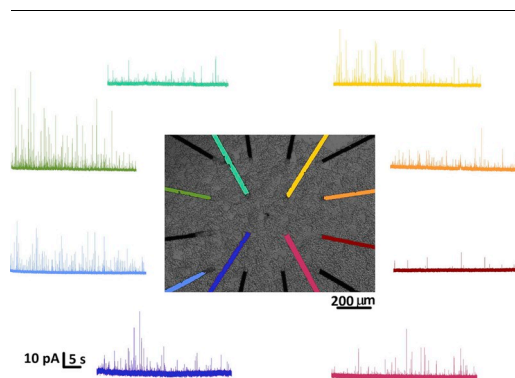
<sup>c</sup> Institute of Electron Devices and Circuits, University of Ulm, 89069 Ulm, Germany



## HIGHLIGHTS

- Simultaneous multisite amperometric recording by means of diamond based MEA sensors
- PC12 secretion modulation through L-DOPA administration
- Evaluation of exocytotic spikes parameters before and after drug injection

## GRAPHICAL ABSTRACT



## ARTICLE INFO

**Keywords:**  
Secretion  
Dopamine  
L-Dopa  
Diamond MEA  
PC12 cells

## ABSTRACT

Micro graphitic – diamond – multi electrode arrays ( $\mu$ G-D-MEAs) are suitable for measuring multisite quantal dopamine (DA) release from PC12 cells. Following cell stimulation with high extracellular KCl and electrode polarization at +650 mV, amperometric spikes are detected with a mean frequency of  $0.60 \pm 0.16$  Hz. In each recording, simultaneous detection of secretory events is occurred in approximately 50% of the electrodes. Kinetic spike parameters and background noise are preserved among the different electrodes. Comparing the amperometric spikes recorder under control conditions with those recorders from PC12 cells previously incubated for 30 min with the dopamine precursor Levodopa (L-DOPA, 20  $\mu$ M) it appears that the quantal size of amperometric spikes is increased by 250% and the half-time width ( $t_{1/2}$ ) by over 120%. On the contrary, L-DOPA has no effect on the frequency of secretory events.

Overall, these data demonstrate that the  $\mu$ G-D-MEAs represent a reliable bio-sensor to simultaneously monitor quantal exocytotic events from different cells and in perspective can be exploited as a drug-screening tool.

## 1. Introduction

Vesicular exocytosis, i.e. the fusion of a secretory vesicle with the

plasma membrane, is a key process regulating synaptic transmission. Both in neurons and neuroendocrine cells,  $Ca^{2+}$ -dependent exocytosis requires that small synaptic vesicles (or dense core vesicles) undergo a

\* Corresponding author.

E-mail address: [giulia.tomagra@unito.it](mailto:giulia.tomagra@unito.it) (G. Tomagra).

<https://doi.org/10.1016/j.bpc.2019.106241>

Received 29 June 2019; Received in revised form 29 July 2019; Accepted 29 July 2019

Available online 31 July 2019

0301-4622/ © 2019 Elsevier B.V. All rights reserved.

series of maturation steps, which include the translocation of the vesicles to the release sites, their docking at the plasma membrane, and their priming, a process that makes vesicles ready for fusion. Finally, the vesicular content is extruded through an aqueous pore connecting the vesicle lumen to the extracellular space [1].

Amperometry provides a fast and real-time measurement of the exocytotic event, confined to those neurotransmitters that are electrochemically oxidizable (dopamine, adrenaline, noradrenaline, serotonin). The amperometric detection of exocytosis requires a suitably polarized sensing electrode is properly polarized to induce the oxidation of released molecules and positioned in close proximity to the cell membrane to fully resolve many secretory events. In this way, released neurotransmitters, reaching in contact with the electrode surface, are oxidized and produce an amperometric spike current of 20–100 pA lasting few ms. Due to the excellent temporal resolution of this technique (sub-millisecond time scale), the distinct kinetic phases of the amperometric event (i.e. the measured spike) can be identified, and the vesicular content of the secretory granule quantified.

Despite carbon fiber microelectrodes (CFEs) represent the gold standard approach for amperometric recordings of quantal release, the increasing need of performing multisite detection and improving the spatial resolution, led to the development of planar multi-arrays, with easily adaptable array geometries and variable dimensions and number of electrodes [2–5].

Several strategies have been developed for the fabrication of multi-electrode arrays with different techniques and different materials. To list a few: platinum ultramicroelectrodes [6], platinum electrodes covered by iridium films [7], sensors based on CNT ITO modified electrodes [8], nitrogen-doped diamond-like-carbon [9], boron-doped diamond [10,11] and Micro Graphitic –Diamond – Multi-Electrode Arrays ( $\mu$ G-D-MEAs) [12–16].

The aim of this work is to demonstrate that the  $\mu$ G-D-MEAs are a valid tool for real-time monitoring of quantal release during cell activity.

## 2. Materials and methods

### 2.1. $\mu$ G-D-MEAs fabrication

Micro Graphitic –Diamond – Multi-Electrode Arrays ( $\mu$ G-D-MEAs) are fabricated in high-quality artificial diamond substrates produced by Chemical Vapor Deposition. The crystals are classified as “type IIa” with the following manufacturing specifications of the substrate:  $4.5 \times 4.5 \times 0.5 \text{ mm}^3$  in size, optically polished on the two opposite large faces. As extensively detailed in previous works [17–19] MeV ion beam lithography (i.e. 1.8 MeV He beam delivering at a fluence of  $1 \times 10^{17} \text{ cm}^{-2}$ ) allows the creation of highly damaged regions embedded in the surrounding diamond matrix. The definition of the

geometry of the implanted regions is obtained by means of a 100  $\mu\text{m}$  thick metal stencil mask which collimates the ion beam, while the modulation of the ion energy (and thus their penetration depth in the sample), is achieved using copper masks with thickness varying in the 0–5  $\mu\text{m}$  range deposited directly over the crystal substrate. After a high-temperature thermal annealing treatment (950 °C in high vacuum for 2 h) the amorphized tracks convert into nanocrystalline graphite if a critical dose was overcome (graphitization threshold  $(5 \div 9) \times 10^{22} \text{ vac cm}^{-3}$ ) [20–22].

This fabrication scheme allows the creation of graphitic micro-channels emerging at the surface of the substrate in correspondence of the desired locations. The implanted graphitic channels have length of  $950 \div 1200 \mu\text{m}$ , width of  $\sim 20 \mu\text{m}$  and thickness of  $\sim 250 \text{ nm}$ , while the electrode active area (emerged cross-section) has a size of  $\sim 100 \mu\text{m}^2$ .

### 2.2. $\mu$ G-D-MEAs – biosensor

The employed biosensors consist of 16 channels multi-electrode arrays allowing the collection of independent and simultaneous amperometric signals from different cells. The chip carrier is equipped with a 1 ml culture chamber with an Ag/AgCl reference electrode. The front-end electronics are based on low-noise transimpedance amplifiers, having an input bias current of 1 pA and the gain set by feedback-resistors of 100 M $\Omega$ . The signals are converted by a USB-6216 ADC module (National Instruments) equipped with Bessel low-pass filters of the sixth order with a bandwidth of 5 kHz. This configuration is optimized for amperometric acquisitions with sampling rate up to 25 kHz. The bias applied to the channels is +650 mV, a value that guarantees the oxidation of the dopamine with an optimal signal-to-noise ratio.

### 2.3. PC12 cell line culture

PC12 cell line derives by pheochromocytoma of the rat adrenal medulla, which was firstly cultured by Greene and Tischler in 1976 [23]. This cell line is often used as a model for study on neurodegenerative pathology such as Parkinson's disease, sharing the mechanism and the neurotransmitters of dopaminergic neurons.

The  $\mu$ G-D-MEAs are coated with collagen type I (Sigma-Aldrich) and placed in an incubator for 1 h; afterwards, the excess of collagen is removed by means of a gentle wash of Phosphate-buffered saline (PBS). PC12 cells are treated with trypsin EDTA (0.25% Sigma-Aldrich) for 8 min to detach them from the surface of the flasks in which are grown; after this step, they are centrifuged and plated in the devices. Cells are maintained in RPMI-1640 (Invitrogen) medium (containing 10% horse serum (Invitrogen), 5% fetal bovine serum (Invitrogen) and 2% antibiotic/antimitotic (pen/strep Invitrogen), at a temperature of 37 °C in a 5% CO<sub>2</sub> atmosphere. The experiments are performed 3/4 days after culturing at room temperature. During the experiments in which

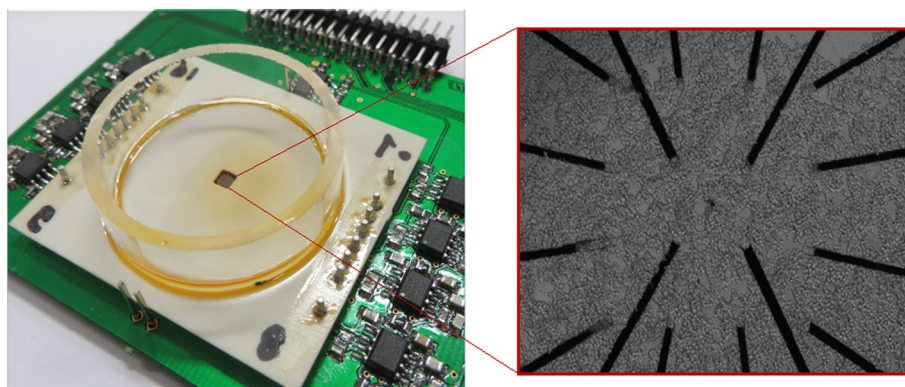
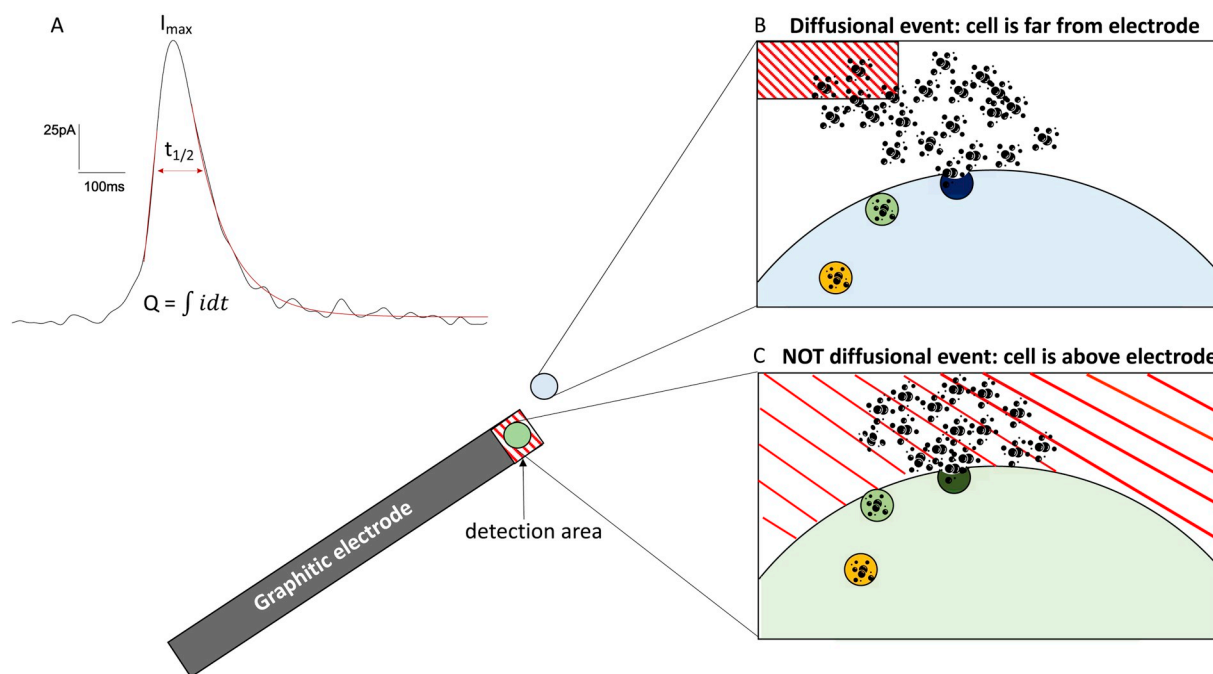
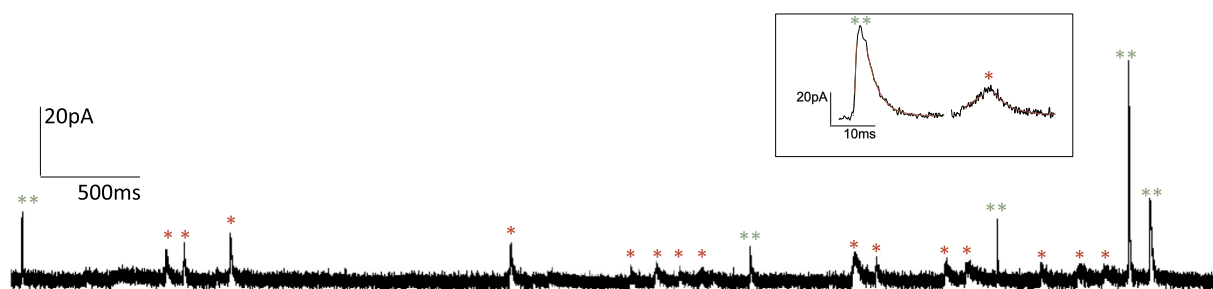


Fig. 1.  $\mu$ G-D-MEA accommodated in the dedicated front-end electronics and micrograph of PC12 cells plated on the sensor.



**Fig. 2.** A. Magnification of a representative spike:  $I_{\max}$  is the maximum of the current generated by the oxidized molecules;  $t_{1/2}$  is the time at which the spike amplitude reaches 50% of its maximum value;  $Q$  is the charge, calculated as the integral of the current over time; rise time of the ascending slope and decrease time (in red in the figure) [30]. B–C. Different positions of the secreting cell respect to the sensing micro-graphitic electrode: the cell is far from the electrode (B), giving rise to the detection of smaller events and diffusional signals. (C) The cell is located above the electrode. (For interpretation of the references to colour in this figure legend, the reader is referred to the web version of this article.)



**Fig. 3.** Representative amperometric recording from one of the 16 micro-graphitic electrodes of the  $\mu$ G-D-MEA. Exocytosis is triggered by dispensing 30 mM KCl. Exocytotic events, associated to the quantal release of dopamine, have been detected as a series of amperometric spikes. The recording lasted several seconds. Diffusional events (rise time  $> 3$  ms) are indicated by red asterisks. Inset: two events shown at higher magnification. (For interpretation of the references to colour in this figure legend, the reader is referred to the web version of this article.)

levodopa (L-DOPA, 20  $\mu$ M) is administered, cells are incubated for 30 min at 37  $^{\circ}$ C, in a 5%  $\text{CO}_2$  humidified atmosphere. Exocytosis is stimulated by applying 30 mM KCl (Fig. 1).

#### 2.4. Amperometric recordings using $\mu$ G-D-MEA

In order to induce dopamine oxidation, a bias ranging between +600 mV and +800 mV [12,24] is applied to the electrodes, with the consequent formation of dopamine-o-quinone and the donation of two electrons, that are detected as an amperometric current by the graphitic electrodes. For each spike, the number of oxidized molecules can be calculated by the Faraday's law, as the time integral of the current transient. The total collected charge is  $Q = \int i dt = Nn_eF$ , where  $N$  is the number of detected moles,  $n_e$  is the number of electrons transferred in the oxidation reaction, and  $F$  is the Faraday's constant [25].

In general, the collection efficiency of an electrode depends from the geometry of electrode and the geometry of releasing cell surface.

Usually, during measurements performed using CFEs, the operator positions the electrode as close as possible to the surface of the cell membrane in order to minimize the effects of diffusion and optimize the collection efficiency of oxidized molecules. On the other hand, the use of planar sensors offers the advantage that the cells are directly plated on the detection spots. The shape of the signal is closely linked to the cell position with respect to the electrode active area since both the width of the spike at half height ( $t_{1/2}$ , half-time width) increase and  $I_{\max}$  (maximum oxidation current) decreases with distance, if secretion events are recorded from cell not properly located on the electrodes active area [26]. In order to exclude diffusional events, spikes with a rise time larger than 3 ms (measured from 25% to 75% of the rising slope) are excluded from the data analysis [27–29]. A representative amperometric spike detected from PC12 cells is shown in Fig. 2A. Diffusional events (discarded from the analysis) versus amperometric spikes, classified on the basis of their rising time, are both visible in Fig. 3.

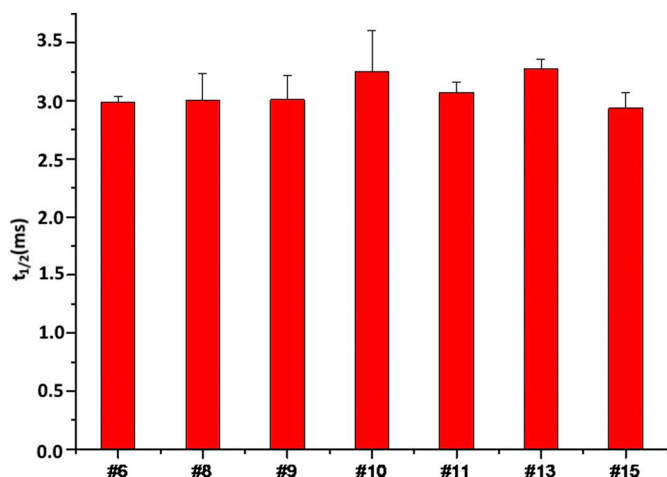


Fig. 4. Analysis on  $t_{1/2}$  parameter variability. No significant differences in data are observed, regardless of the sensing electrode.

### 3. Results

#### 3.1. Multisite amperometric recordings before and after L-DOPA incubation

The major advantage of performing real-time measurement using multi-arrays is to simultaneously measure the secretion from multiple cells. In order to compare the responsiveness of 7 test electrodes, we compared among them the mean values of a kinetic spike parameter

( $t_{1/2}$ ,  $(3.1 \pm 0.4)$  ms) and of the basal current noise ( $(5.8 \pm 0.2)$  pA,  $n = 16$  electrode, figure not showed). In Fig. 4 it is possible to observe that the mean  $t_{1/2}$ , independently of the electrode and the device from which the signal is collected, does not exhibit any statistically significant variations, ( $p > .05$ , ANOVA Bonferroni post-hoc comparison).

Fig. 5A shows a typical recording of amperometric spikes using a  $\mu$ G-D-MEA. The secretory activity of several PC12 cells is recorded from 13 out of the 16 electrodes, allowing to collect a significant number of events in few recordings (i.e.  $n \geq 1500$  events/device). After recording under control conditions (external stimulation with 30 mM KCl), PC12 cells are incubated with the dopamine precursor L-3, 4-dihydroxyphenylalanine (L-DOPA), to increase the dopamine content [31]. The effect of the treatment with L-DOPA is shown for a representative electrode in Fig. 5B. We found that the frequency of amperometric spikes generation is not affected by L-DOPA [32] ( $(0.60 \pm 0.16)$  Hz in control condition and  $(0.56 \pm 0.12)$  Hz after L-DOPA incubation,  $p > .1$ ), and that the  $\text{Ca}^{2+}$  channel blocker  $\text{CdCl}_2$  ( $500 \mu\text{M}$ ), completely suppressed the exocytotic response. On the contrary, L-DOPA caused a significant increase in the number of secreted molecules (250% with respect to control,  $p < .05$ ). The mean values of the spike charge ( $Q$ ) increased from  $(0.143 \pm 0.002)$  pC (control) to  $(0.320 \pm 0.010)$  pC (L-DOPA) ( $p < .05$ ). Similarly, concerning the kinetic spike parameters, that the  $t_{1/2}$  is increased by over 120% with respect to control condition, i.e. from  $(2.79 \pm 0.03)$  ms to  $(6.01 \pm 0.18)$  ms ( $p < .05$ ). These findings are in good agreement with those reported by Pothos et al. [32], thus confirming the reliability of  $\mu$ G-D-MEAs.

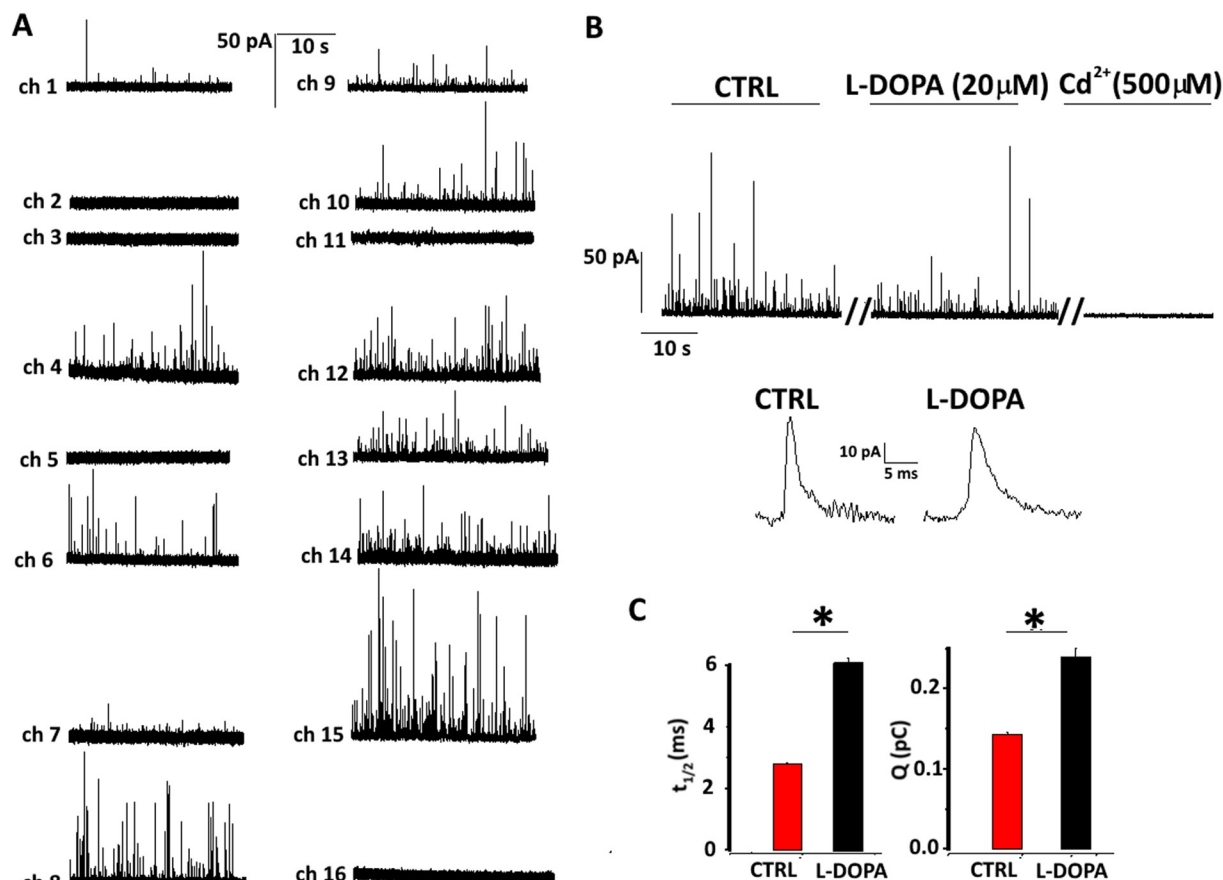
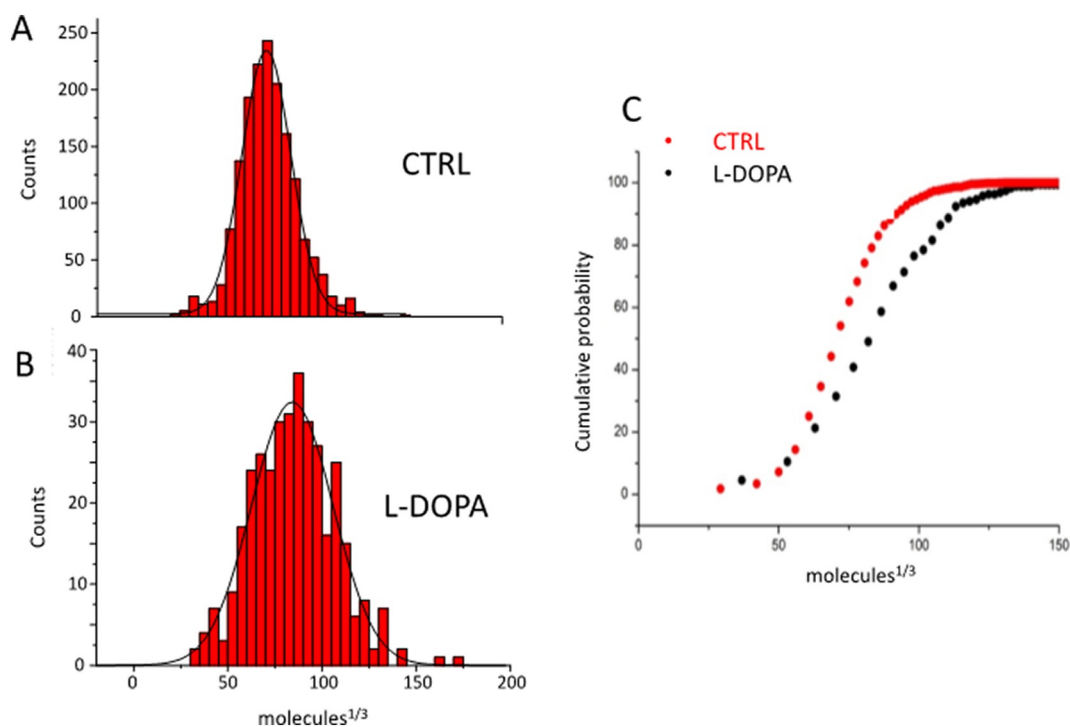


Fig. 5. A. Amperometric recordings from 16 different electrodes. B. A representative trace in control condition, after incubation with L-DOPA for 30 min and in the presence of  $\text{Cd}^{2+}$  ( $500 \mu\text{M}$ ). Inset: magnification of two amperometric spikes, in control conditions and following L-DOPA incubation. C. Histograms of half-height width and relative charge in control and after incubation with L-DOPA.



**Fig. 6.** A: cumulative probability of the molecules<sup>1/3</sup>, in control and after incubation with L-DOPA, the curve with L-DOPA is displaced to higher values. B-C: the typical probability distribution, in control (B) and with L-DOPA (C), the L-DOPA distribution sharply spikes to the left, on values greater than the control, confirming what is observed in the curve of the cumulative probabilities.

### 3.2. Distribution of quantal size variability, in control and with L-dopa

The distribution of the vesicles radii derives from molecule<sup>1/3</sup> values using the Farady law [33], assuming spherical shape of the vesicles [34].

The cube root of the quantal size before and after L-DOPA is normal distributed (Fig. 6B, C), as confirmed from the determination coefficient calculated from the fit ( $R_{CTRL} = 0.99$ ;  $R_{L-DOPA} = 0.96$ ). The entire population of quanta after L-DOPA treatment is significantly shifted to larger values with respect to control ( $p < .05$ , KS test = 0.79). The corresponding cumulative distributions is shown in Fig. 6C, where is evident that the distribution with L-DOPA is shifted by 17% toward higher values with respect to control (peak  $\max_{CTRL} = (71.9 \pm 0.3)$  pA, peak  $\max_{L-DOPA} = (84.2 \pm 0.7)$  pA) [35–37].

These results, using the  $\mu$ G-D-MEA, confirm that incubating with L-DOPA increases the quantum release of dopamine.

## 4. Discussion

Here we demonstrated that  $\mu$ G-D-MEAs are as efficient as CFEs to monitor in real-time the exocytotic activity of PC12 cells. As PC12 cells are cultured on the  $\mu$ G-D-MEA surface, amperometric detection can be simultaneously performed by 16 graphitic electrodes: this implies speeding up of data acquisition and avoiding mechanical cell stimulation.

Moreover,  $\mu$ G-D-MEAs are reliable devices to carry out pharmacological studies, targeted to monitor alterations in the kinetics and amplitude of quantal secretory events. For example, we have shown that incubating the cells with L-DOPA causes significant changes in the shape of the amperometric spikes. These results are consistent with those performed by Pothos et al. [32]. In the cited work, 1 h incubation with 50  $\mu$ M of L-DOPA potentiated by 250% the quantal release; in our case, we have incubated PC12 cells for 1 h at 20  $\mu$ M and we have obtained an increment of 120%.

The reason for this change in the shape of the spikes is rather

complex [38], nonetheless some hypotheses can be advanced. Sombers et al. [38] hypothesized that L-DOPA favors multiple pre-fusion events (i.e. fusion between two or more vesicles before exocytosis). Alternatively, Colliver et al. [39] from TEM images observed that after incubation with L-DOPA there is a significant increase in the diameter and volume of the vesicles, these pharmacological studies demonstrated that this increase is mediated by the vesicular monoamine transporter (VMAT).

## Acknowledgment

Stock PC12 cells were generously provided by Dr. R.H.S. Westerink (Utrecht university).

This work was supported by the following projects: Project 2015FNWP34 (from Italian MIUR, Italy) V.C. and CSTO165284 (from Compagnia di San Paolo, Italy) to V.C.

F.P. and P.O. gratefully acknowledge the support of the following projects: DIACELL project (funded by the National Institute of Nuclear Physics, Italy), MiRaDS project (funded by CRT Foundation, Italy), “Finanziamento ex-post di progetti di ricerca di Ateneo” (funded by Compagnia di SanPaolo Foundation), “Departments of Excellence” (L. 232/2016) project (funded by Italian MIUR, Italy). Ion beam irradiations were performed at the AN2000 accelerator of the Legnaro National Laboratories of the Italian Institute of Nuclear Physics (INFN) within the “Dia.Fab.” beamtime.

## Appendix A. Supplementary data

Supplementary data to this article can be found online at <https://doi.org/10.1016/j.bpc.2019.106241>.

## References

- [1] F. Lemaître, M. Guille Collignon, C. Amatore, Recent advances in electrochemical detection of exocytosis, *Electrochim. Acta* (2014), <https://doi.org/10.1016/j.electacta.2014.02.059>.

- [2] V. Carabelli, et al., Planar diamond-based multiarrays to monitor neurotransmitter release and action potential firing: new perspectives in cellular neuroscience, *ACS Chem. Neurosci.* (2017), <https://doi.org/10.1021/acschemneuro.6b00328>.
- [3] K.D. Gillis, X.A. Liu, A. Marcantoni, V. Carabelli, Electrochemical measurement of quantal exocytosis using microchips, *Pflugers Archiv European Journal of Physiology* (2018), <https://doi.org/10.1007/s00424-017-2063-2>.
- [4] A. Pasquarelli, F. Picollo, V. Carabelli, Boron-doped diamond and graphitic multi-arrays for neurotransmitter sensing, in: Springer (Ed.), *Carbon-Based Nanosensor Technol.* Springer Ser. Chem. Sensors Biosens. Methods Appl, 2018, [https://doi.org/10.1007/5346\\_2018\\_24](https://doi.org/10.1007/5346_2018_24).
- [5] G. Tomagra, et al., Quantal release of dopamine and action potential firing detected in midbrain neurons by multifunctional diamond-based microarrays, *Front. Neurosci.* (2019), <https://doi.org/10.3389/fnins.2019.00288>.
- [6] S.Y. Yang, et al., Detection of transmitter release from single living cells using conducting polymer microelectrodes, *Adv. Mater.* (2011), <https://doi.org/10.1002/adma.201100035>.
- [7] I.A. Ges, R.L. Brindley, K.P.M. Currie, F.J. Baudenbacher, A microfluidic platform for chemical stimulation and real time analysis of catecholamine secretion from neuroendocrine cells, *Lab Chip* (2013), <https://doi.org/10.1039/c3lc50779c>.
- [8] B.X. Shi, Y. Wang, K. Zhang, T.L. Lam, H.L.W. Chan, Monitoring of dopamine release in single cell using ultrasensitive ITO microsensors modified with carbon nanotubes, *Biosens. Bioelectron.* (2011), <https://doi.org/10.1016/j.bios.2010.11.037>.
- [9] Y. Gao, X. Chen, S. Gupta, K.D. Gillis, S. Gangopadhyay, Magnetron sputtered diamond-like carbon microelectrodes for on-chip measurement of quantal catecholamine release from cells, *Biomed. Microdevices* (2008), <https://doi.org/10.1007/s10544-008-9173-8>.
- [10] S. Gosso, et al., Heterogeneous distribution of exocytotic microdomains in adrenal chromaffin cells resolved by high-density diamond ultra-microelectrode arrays, *J. Physiol.* (2014), <https://doi.org/10.1113/jphysiol.2014.274951>.
- [11] J. Park, J.J. Galligan, G.D. Fink, G.M. Swain, In vitro continuous amperometry with a diamond microelectrode coupled with video microscopy for simultaneously monitoring endogenous norepinephrine and its effect on the contractile response of a rat mesenteric artery, *Anal. Chem.* (2006), <https://doi.org/10.1021/ac060440u>.
- [12] F. Picollo, et al., Development and characterization of a diamond-insulated graphitic multi electrode array realized with ion beam lithography, *Sensors (Switzerland)* (2015), <https://doi.org/10.3390/s150100515>.
- [13] F. Picollo, et al., A new diamond biosensor with integrated graphitic microchannels for detecting quantal exocytotic events from chromaffin cells, *Adv. Mater.* (2013), <https://doi.org/10.1002/adma.201300710>.
- [14] F. Picollo, et al., All-carbon multi-electrode array for real-time in vitro measurements of oxidizable neurotransmitters, *Sci. Rep.* (2016), <https://doi.org/10.1038/srep20682>.
- [15] F. Picollo, et al., Microelectrode arrays of diamond-insulated graphitic channels for real-time detection of exocytotic events from cultured chromaffin cells and slices of adrenal glands, *Anal. Chem.* 88 (2016) 7493–7499.
- [16] G. Tomagra, et al., Micro graphite-patterned diamond sensors: towards the simultaneous in vitro detection of molecular release and action potentials generation from excitable cells, *Carbon N. Y.* 152 (2019) 424–433.
- [17] F. Picollo, et al., Formation of buried conductive micro-channels in single crystal diamond with MeV C and He implantation, *Diam. Relat. Mater.* 19 (2010) 466–469.
- [18] F. Picollo, et al., Realization of a diamond based high density multi electrode array by means of deep ion beam lithography, *Nucl. Instruments Methods Phys. Res. Sect. B Beam Interact. with Mater. Atoms* 348 (2015) 199–202.
- [19] F. Picollo, et al., Fabrication and electrical characterization of three-dimensional graphitic microchannels in single crystal diamond, *New J. Phys.* 14 (2012) 053011.
- [20] A. Battiato, et al., Softening the ultra-stiff: controlled variation of Young's modulus in single-crystal diamond by ion implantation, *Acta Mater.* 116 (2016) 95–103.
- [21] D.P. Hickey, K.S. Jones, R.G. Elliman, Amorphization and graphitization of single-crystal diamond - a transmission electron microscopy study, *Diam. Relat. Mater.* 18 (2009) 1353–1359.
- [22] C. Uzansaguy, et al., Damage threshold for ion-beam-induced graphitization of diamond, *Appl. Phys. Lett.* 67 (1995) 1194–1196.
- [23] L.A. Greene, A.S. Tischler, Establishment of a noradrenergic clonal line of rat adrenal pheochromocytoma cells which respond to nerve growth factor, *Proc. Natl. Acad. Sci. U. S. A.* 73 (7) (1976) 2424–2428.
- [24] G. Tomagra, et al., Diamond-based multi electrode arrays for monitoring neurotransmitter release, *Lecture Notes in Electrical Engineering* 539 (2019).
- [25] D. Bruns, Detection of transmitter release with carbon fiber electrodes, *Methods* (2004), <https://doi.org/10.1016/j.ymeth.2004.01.004>.
- [26] T.K. Chen, G. Luo, A.G. Ewing, Amperometric monitoring of stimulated catecholamine release from rat Pheochromocytoma (PC12) cells at the Zeptomole level, *Anal. Chem.* (1994), <https://doi.org/10.1021/ac00091a007>.
- [27] E.V. Mosharov, D. Sulzer, Analysis of exocytotic events recorded by amperometry, *Nat. Methods* (2005), <https://doi.org/10.1038/nmeth782>.
- [28] F. Segura, M.A. Brioso, J.F. Gómez, J.D. Machado, R. Borges, Automatic analysis for amperometric recordings of exocytosis, *J. Neurosci. Methods* (2000), [https://doi.org/10.1016/S0165-0270\(00\)00309-5](https://doi.org/10.1016/S0165-0270(00)00309-5).
- [29] J.F. Gómez, M.A. Brioso, J.D. Machado, J.L. Sánchez, R. Borges, New approaches for analysis of amperometric recordings, *Annals of the New York Academy of Sciences*, 2002, <https://doi.org/10.1111/j.1749-6632.2002.tb04544.x>.
- [30] A. Meunier, et al., Amperometric detection of vesicular exocytosis from BON cells at carbon fiber microelectrodes, *Electrochim. Acta* (2014), <https://doi.org/10.1016/j.electacta.2013.07.110>.
- [31] K.D. Kozminski, D.A. Gutman, V. Davila, D. Sulzer, A.G. Ewing, Voltammetric and pharmacological characterization of dopamine release from single exocytotic events at rat pheochromocytoma (PC12) cells, *Anal. Chem.* (1998), <https://doi.org/10.1021/ac980129f>.
- [32] E. Pothos, M. Desmond, D. Sulzer, L-3,4-Dihydroxyphenylalanine increases the quantal size of Exocytotic dopamine release in vitro, *J. Neurochem.* (2002), <https://doi.org/10.1046/j.1471-4159.1996.66020629.x>.
- [33] J.A. Jankowski, T.J. Schroeder, E.L. Ciolkowski, R.M. Wightman, Temporal characteristics of quantal secretion of catecholamines from adrenal medullary cells, *J. Biol. Chem.* 268 (20) (1993) 14694–14700.
- [34] A. Marcantoni, V. Carabelli, D.H. Vandael, V. Comunanza, E. Carbone, PDE type-4 inhibition increases L-type Ca<sup>2+</sup> currents, action potential firing, and quantal size of exocytosis in mouse chromaffin cells, *Pflugers Arch. Eur. J. Physiol.* (2009), <https://doi.org/10.1007/s00424-008-0584-4>.
- [35] J.M. Bekkers, C.F. Stevens, Presynaptic mechanism for long-term potentiation in the hippocampus, *Nature* (1990), <https://doi.org/10.1038/346724a0>.
- [36] E.N. Pothos, V. Davila, D. Sulzer, Presynaptic recording of quanta from midbrain dopamine neurons and modulation of the quantal size, *J. Neurosci.* 18 (11) (1998) 4106–4118.
- [37] M.A. Mena, V. Davila, J. Bogalovsky, D. Sulzer, A synergistic neurotrophic response to l-dihydroxyphenylalanine and nerve growth factor, *Mol. Pharmacol.* 54 (4) (1998) 678–686.
- [38] L.A. Sombers, The effects of vesicular volume on secretion through the fusion pore in Exocytotic release from PC12 cells, *J. Neurosci.* (2004), <https://doi.org/10.1523/jneurosci.1119-03.2004>.
- [39] T.L. Collier, S.J. Pyott, M. Achalabun, A.G. Ewing, VMAT-mediated changes in quantal size and vesicular volume, *J. Neurosci.* 20 (14) (2000) 5276–5282.